Dalton Transactions

Accepted Manuscript

This article can be cited before page numbers have been issued, to do this please use: H. Huo, X. Xu, T. Zhao, Y. Li, Y. Jiang and K. Lin, *Dalton Trans.*, 2018, DOI: 10.1039/C7DT04832G.

ROYAL SOCIETY OF CHEMISTRY

rsc.li/dalton

View Article Online
DOI: 10.1039/C7DT04832G

Journal Name

ARTICLE

Hybrid mesoporous organosilicas with molecularly imprinted cavities: towards extended exposure of active amino groups in the framework wall

Received 00th January 20xx,
Accepted 00th January 20xx

DOI: 10.1039/x0xx00000x

www.rsc.org/

Hang Huo[a], Xianzhu Xu[a], Tingting Zhao[a], Yudong Li[a], Yanqiu Jiang*[a] and Kaifeng Lin*[a,b]

Hybrid molecularly imprinted mesoporous silica were synthesized by co-condensation of tetraethoxysilane and functional organosilica precursors of HQP and BPAP, in which hydroquinone (HQ) and bisphenol A (BPA) were linked as imprinting molecules. Owing to the existence of thermally reversible covalent bond of carbamate (-NH-COO-), the imprinting molecules could be eliminated under thermal treatment and molecularly imprinted cavities were formed in framework wall. All of these materials were used to catalyze heterogeneous Knoevenagel reactions and proved to exhibit higher catalytic conversion and turnover frequency (TOF) number compared with the materials with imprinting molecules, which is attributed to the presence of amino groups with higher basicity and molecularly imprinted cavities. Importantly, compared with amino functionalized SBA-15 materials, the decisive role of molecularly imprinted cavities on the enhanced accessibility of amino groups in mesoporous framework was further confirmed. Moreover, the size of imprinting molecules has an influence on the catalytic conversion and TOF values: imprinting molecules with relatively bulkier size tend to lead higher accessibility to the active sites. The amino groups in the framework are extremely stable during the reaction procedure and recycle process.

Introduction

Silica oxide based mesoporous materials as a branch of inorganic molecular sieves have potential industrial application in the fields of catalysis[1-4], drug or gene delivery[5], chromatography[6] and adsorption[7] due to their biocompatibility, large specific surface area, tunable pore size and thermal stability. In the year of 1999, periodic ordered mesoporous organosilicas (PMOs) were first synthesized via the co-condensation of inorganic silica species and bridged organosilica precursors $[(RO)_3Si\text{-}R\text{-}Si(OR)_3]$[8, 9], which were homogeneously distributed in the three dimensional framework. As a novel concept, the development of PMOs was promising and rapid[10]. A range of organic functional groups were successfully incorporated into the framework of the materials, including ionic liquid[11, 12], alkane, aromatic benzene derivatives[13], cyclohexane-diamine[14], binol[15] or even a metallic center chelating to an organic ligand, as salon skeleton[16, 17]. In addition to adjusting the linkage of silica blocks, decorating the organosilica precursors with alcohols[18], thiols[19], sulfonic[20], chiral groups[21] and acid or base species[22, 23] also makes it possible to the successful synthesis of PMOs. The combination of robust inorganic framework and active organic species tremendously enriches the diverse application of the materials, for instance, enzyme immobilization[24], chiral separation[6], photochemistry[25, 26] and acid/base catalysis[13, 27, 28].

In the field of catalysis, PMO materials show perfect catalytic performance as their large surface area, ordered porous structure, thermal stability and abundant active species. However, it should be taken into account that traditional PMO may suffer from a kind of shortcoming that the access of reactants to the active species is limited to a certain extent because some of the active species are buried in the framework of the material. This kind of limitation can be amplified when the bonding of active species and the framework wall is rigid and the pore distribution is narrow[29]. An alternative way to overcome this problem is post-grafting method, by which organic active species are anchored to outer surface or internal channels of pre-synthesized silica matrix[30-32]. In certain cases, however, some of the pores may be more or less blocked by organic species when they are tethered in the channels[33-35], which makes those pores inaccessible to reactants due to the diffusion limitation. So it is still necessary to pay more effort to explore an effective method to overcome these weaknesses.

Molecular imprinting is known as a technology that can contribute molecularly imprinted cavities in a solid polymer matrix to recognize template molecules or their analogues by covalence/non-covalence interaction or hydrogen bond. Up to now, molecularly imprinted materials have been widely used in the field of heterogeneous catalysis[36, 37], sustained release drugs[38, 39], chemical bionic sensor[40], exclusive adsorption and separation[41,42]. It

[a]School of Chemistry and Chemical Engineering, Harbin Institute of Technology, Harbin, Heilongjiang, 150001, P. R. China.
[b]Key laboratory of Advanced Energy Materials Chemistry (Ministry of Education), Nankai University, Tianjin, 30071, P. R. China.
E-mail: jiangyanqiu@hit.edu.cn; linkaifeng@hit.edu.cn.
Electronic Supplementary Information (ESI) available: Fig. S1-S8, Scheme S1 and Table S1. See DOI: 10.1039/x0xx00000x

View Article Online
DOI: 10.1039/C7DT04832G

has been reported that the active sites buried in solid polymers are inactive[36], whereas molecularly imprinted cavities in the materials make these active sites accessible to the reactants. Therefore, introducing some molecularly imprinted cavities nearby active sites in framework of PMO is reasonably expected to make an effort towards extended exposure of the active sites located in the framework, thus resulting in the enhanced accessibility. It is worth noting that such molecularly imprinted mesoporous organosilicas can be prepared using a semi-covalent imprinting technique. On such materials, a study has also been performed to compare materials imprinted with a range of molecularly imprinted cavities of varying size in mesoporous silicas and their recognizing properties for different imprinting molecules. Although such molecularly imprinted materials have not been devoted to apply as heterogeneous catalysts, the study inspired us a useful technique to prepare molecularly imprinted mesoporous organosilicas.

In our study, we prepared a series of molecularly imprinted hybrid mesoporous materials using hydroquinone (HQ) and bisphenol A (BPA) as imprinting molecules via a triblock copolymer templated sol-gel approach. Removing the imprinting molecules by thermal treatment in DMSO yields novel materials with molecularly imprinted cavities and functional amino groups in the framework. It is worth noting that based on the fact that most of the amino groups can be exposed in the molecularly imprinted cavities and no organic groups occupy the mesopore channels, such hybrid materials showed enhanced catalytic performance in heterogeneous Knoevenagel reactions compared with the materials containing imprinting molecules in the framework wall and the traditional amino functionalized one-pot synthesized or post-grafted SBA-15 materials.

Experimental Section

Chemical reagents

(3-Isocyanatopropyl) triethoxysilane (ICPTES), hydroquinone and bisphenol A were purchased from Aladdin Industrial Corporation and used without further purification. tetraethoxysilane (TEOS) was obtained from Sinopharm Chemical Reagent Beijing Co., Ltd. PluronicP123 (P123, $EO_{20}PO_{70}EO_{20}$) was purchased from Aldrich. All chemical reagents were used as received.

Preparation of organosilica precursors of HQP and BPAP

The organosilica precursors were synthesized according to previously reported method[43] and the synthesis process is illustrated in **Scheme 1**. Typically, the hydroquinone-based organosilica precursor (HQP) was synthesized as follows: hydroquinone (HQ, 15 mmol) and (3-Isocyanatopropyl) triethoxysilane (ICPTES, alkoxysilane monomer; 30 mmol) were added to 20 mL of absolute tetrahydrofuran (THF) in a round-bottomed flask with a magnetic stirrer, and the reaction proceeded under an inert atmosphere at the temperature of 65°C for 24 h. After the reaction, the volatile solvent of THF was evaporated by a rotary evaporator. The crude product was purified by washing with 20 mL of hexane and recrystallized in solvent of

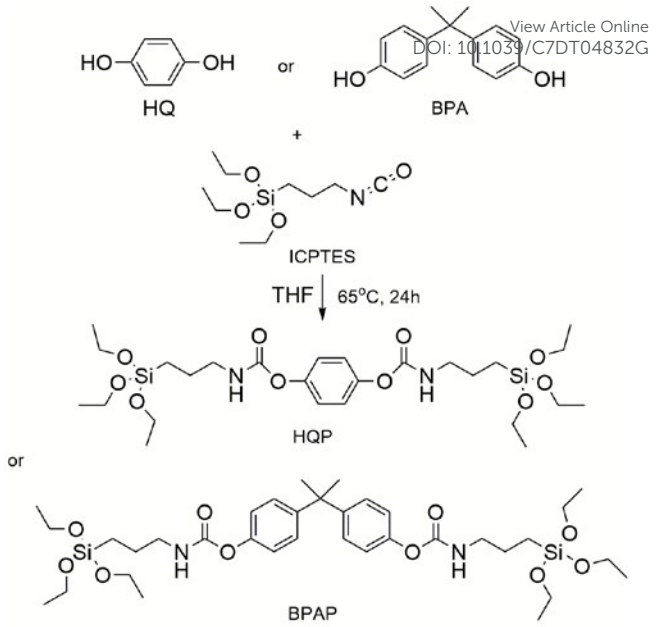

Scheme 1 Synthesis of HQP/BPAP with HQ/BPA and ICPTES in stoichiometric ratio

methanol. Then, removing the solvent in vacuum gets the product as a white powder, and the yield is 91%. The ^{1}H NMR spectrum is shown in **Fig. S1A**. Bisphenol A-based organosilica precursor (BPAP) was synthesized in a similar way with bisphenol A (BPA, 15 mmol) and 3-Isocyanatopropyltriethoxysilane (ICPTES, 30 mmol) as starting materials, and the reaction was carried out in THF and refluxed for 24 h under an inert atmosphere. The BPAP was obtained with yield of 87% as a white powder and its ^{1}H NMR spectra is shown in **Fig. S1B**.

Preparation of molecularly imprinting mesoporous silica of MIMS-NHQ and MIMS-NBPA

In the molecularly imprinted mesoporous silica materials, the imprinting molecules of HQ and BPA are covalent bonded with the –NH-CO- group, and they are denoted as MIMS-NHQ/NBPA (x) (x represents the molar ratio of TEOS and HQP or BPAP, and x= 7, 10, 14 for HQP or x= 14 for BPAP). Here the characters of "NHQ" (or "NBPA") mean that the imprinting molecules of HQ (or BPA) are contained in the materials and linked to thecarbamate (-NH-COO-) bond. These materials are synthesized by the co-condensation of organosilica precursor and TEOS in the presence of triblock copolymer P123 as template under acidic condition. In a typical preparation method for MIMS-NHQ (14), 0.8g of P123 was dissolved in 25 mL pH= 1.5 HCl solution at the temperature of 40°C for 12 h. Afterwards, 1.5 mL of TEOS and 0.29 g of HQP precursor dissolving in 1.0 mL of ethanol were added to the solution in dropwise and stirred at 40°C for 24 h. Finally, the suspension was aged at 100°C for 48 h in a sealed PTFE autoclave. The surfactant was removed by refluxing with 85 mL of a mixture (ethanol/HCl; 80:5, v/v) for 24 h. After filtration and being washed thoroughly with deionized water, a white powder was obtained. MIMS-NHQ (10), MIMS-NHQ (7) and MIMS-NBPA (14), were synthesized in the same waywith 0.41 g HQP, 0.54 g HQP, 0.35 g BPAP, respectively. In

these cases, the imprinting molecules (HQ and BPA) were incorporated in the mesoporous framework wall.

Preparation of molecularly imprinting mesoporous silica of MIMS-HQ and MIMS-BPA

The materials with molecularly imprinted cavities in framework were synthesized with thermal treatment of MIMS-NHQ/NBPA (x) by refluxing in DMSO to remove imprinting molecule HQ or BPA, and the materials are designated as MIMS-HQ/BPA (x) (x represents the molar ratio of TEOS and HQ/BPA, and x=7, 10, 14 respectively). In a typical procedure, to a round-bottomed flask, MIMS-NHQ (14) was suspended in a solution of 60 mL dimethylsulfoxide (DMSO) and 5 mL deionized water. Then the mixture was heated with stirring for 6 hours at 165°C. After such thermal treatment, the imprinting molecules (HQ and BPA) were removed and the terminal amino groups and molecularly imprinted cavities were formed in the mesoporous framework wall. The thermal-treated mesoporous materials were isolated by filtration, washed with deionized water and ethanol and dried in vacuum oven at 60°C for 6 h, leading to the formation of the resultant materials of MIMS-HQ (7), MIMS-HQ (10), MIMS-HQ (14) and MIMS-BPA (14).

Characterization

Solution ^{1}H NMR spectrums of HQP and BPAP in $CDCl_3$ were obtained at 25°C on Bruker-400 MHz spectrometer using $CDCl_3$ as solvent and TMS as internal standard. ^{29}Si (79.4 MHz) CP-MAS NMR was obtained on Bruker-AVANCE III-400 WB spectrometer with samples packed in ZrO_2 rotator with KeI-F cap spinning at 8 kHz. The X channel of the 4 mm standard bore CP MAS probehead was tuned to 79.5 MHz for ^{29}Si and the other channel was tuned to 400.18 MHz for broad band ^{1}H decoupling, at a magnetic field of 9.39T of 297 K with the contact time of 2 ms. All ^{29}Si CP-MAS chemical shifts are referenced to the resonances of 3-(trimethylsilyl)-1-propanesulfonic acid salt standard. FT-IR spectrum was obtained, using the KBr buffer technique, on Perkin-Elmer Spectrum 100 spectrometer in the wavenumber range from 4000 to 400 cm^{-1}. Powder XRD was recorded on Bruker -D8 ADVANCE diffractometer with a Ni-filtered Cu-Kα (λ= 1.5418 Å) radiation operating at 40 kV and 30 mA in the 2θ range from 0.8° to 6°. The nitrogen adsorption-desorption measurement was carried out at 77 K on ASAP 2000 system and the specific surface area and pore distribution were calculated from the adsorption isotherm by using Brunauer-Emmet-Teller (BET) and Barrett-Joyner-Halenda (BJH) methods, respectively. For all of the materials, the average pore size was estimated from the pore size distribution curve at the maximum point. TG/DTA analysis was recorded on TA-SDT Q600 analyzer under air condition with the temperature range from 30°C to 800°C. C, H and N elemental analysis was recorded on PerkinElmer PE 2400II, and each sample was tested for twice. SEM and TEM images were recorded on Hitachi SU8010 series and Hitachi H-7650 electron microscope, respectively. A UV-Vis spectrophotometer (BLV-GHX-V, Bilang Corporation, China) was utilized to detect the concentration of imprinting molecules in the adsorption experiment.

The carbon dioxide chemisorption was conducted on a Micromeritics AutoChem 2920 instrument with a TCD detector. The typical CO_2 chemisorption was carried out as follows: about 100 mg of sample was heated to 100°C under helium atmosphere and kept for 20 minutes. Then the temperature was cooled to 75°C, CO_2 chemisorption was performed with a flow of 10 ml/min for 30 minutes. When the temperature was reduced to 30°C, the desorption was executed by purging helium gas at rate of 50 mL/min and ramping the temperature from 30 to 100°C at a rate of 5°C/min and holding at 100°C for 30 minutes. The CO_2 uptake was calculated on the basis of the desorption curve.

Adsorption of imprinting molecules with the material as a solid absorbent

The static adsorption experiments were carried out as following: 20.0 mg of MIMS-HQ (14) was mixed with 3.0 mL HQ solution at concentration of 1.5 mmol L^{-1} in n-hexane/n-propanol (95:5, v/v). The mixtures were stirred at 150 rpm for 20 h at 25°C. After binding, the mixtures were filtered through a 0.22 μm membrane, and the concentration of the filtrates were determined by UV- vis characterization. MIMS-BPA (14) was conducted in the same treatment for the adsorption experiment except with a solution of BPA. At the same time, we also used a sample that was synthesized only with inorganic precursor TEOS (the sample was designated as SBA-15) for comparison. The adsorption capacity was calculated according to the following equation:

$$Q = \frac{(C_0 - C_f) * v}{m}$$

where C_0 (mmol L^{-1}) and C_f (mmol L^{-1}) are the initial and final concentration of template molecules, v (L) is the total volume of the solution, m (g) is the mass of the sorbent, Q is the amount of template molecules adsorbed, respectively.

Catalytic procedure of Knoevenagel reaction

In a typical procedure, the reaction mixture consisted of 40 mg of catalyst, 2 mL of absolute toluene, 1 mmol of ethyl cyanoacetate and 1 mmol of p-Anisaldehyde was allowed to reflux at 110°C for 3 hours. After cooling to room temperature, the catalyst was separated from the reaction mixture via centrifugation and the liquid was analyzed on a gas chromatograph instrument (7890A with FID detector) with n-Butanol as internal standard substance. The assignment of the products was further confirmed by GC-MS experiment. Similarly, the blank comparison experiment was carried out in the same condition except the addition of catalyst.

Results and discussion

Synthesis of the materials

Preparation of MIMS-NHQ and MIMS-NBPA materials containing HQ and BPA units as imprinting molecules was accomplished following a procedure similar to the synthesis of hybrid organic incorporated mesoporous SBA-15 material. At first, HQ and BPA molecules were covalent condensed with ICPTES to form organosilica precursors HQP and BPAP. Subsequently, the silylated

precursors were combined with TEOS in the synthesis of MIMS-NHQ and MIMS-NBPA, using P123 as structure directing agent.

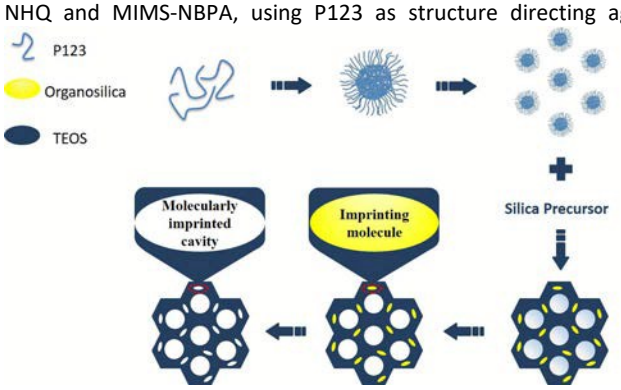

Scheme 2 Possible procedure for fabricating the hybrid mesoporous materials with molecularly imprinted cavities

Materials of MIMS-HQ and MIMS-BPA were derived from MIMS-NHQ and MIMS-NBPA as the carbamate group in HQP and BPAP can thermally decompose to amino group with water.

According to the synthesis of SBA-15 type materials, it is possible to propose a route for fabrication of the hybrid molecularly imprinted materials and the materials with cavities in the mesoporous framework wall (Scheme 2). Under acidic condition, TEOS and organosilica precursors hydrolysed and co-condensed synergistically to construct 2D hexagonal *p6mm* structure with imprinting molecules in the framework, in which P123 was used as structure directing agent. Then, the materials with molecularly imprinted cavities andextended exposure of amino groups in the framework wall were obtained via crystalization and removal of P123 followed by being heated in DMSO. During the thermal treatment at 165°C, the covalent incorporated HQP and BPAP can decomposed into HQ/BPA and ICPTES. In a further step, the ICPTES moiety can hydrolysis with adventitious water into amine and CO_2, leading to the functional organic group in the molecularly imprinted cavities. The react procedure was illustrated in Scheme S1 in supporting information. In sol-gel procedure, the precursor species and ratio of organosilica precursors have an effect on the morphology, mesopore structure and mesopore ordering of the terminal materials.

Characterization of the materials

The chemical composition of the molecularly imprinted hybrid materials and non-imprinted materials was characterized by FT-IR spectroscopy. The FT-IR spectrum of molecularly imprinted hybrid material MIMS-NHQ (14) shows two peaks at 1720 cm^{-1} and 1503 cm^{-1} stretching vibrations of C=O bond in carbamate and C-H bond in benzene moiety, respectively. After thermal treatment, both of the two stretching vibrations disappear and a bending vibration emerges at 1670 cm^{-1} for NH_2 group (Fig. 1 left). The same vibration characters have also been observed in the case of MIMS-NBPA (14) and the thermal treatment also works for creation of amino groups in MIMS-BPA (14) (Fig. 1 right). All of the results indicate that the organosilica precursors were successfully embedded into the framework of mesoporous materials. Being heated in DMSO at

View Article Online
DOI: 10.1039/C7DT04832G

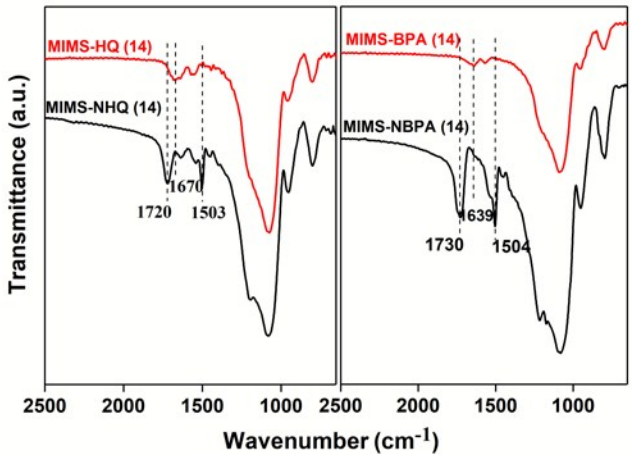

Fig. 1 FT–IR spectra of MIMS-NHQ (14), MIMS-HQ (14) (left) and MIMS-NBPA (14), MIMS-BPA (14) (right)

165°C, the carbamate group of HQP/BPAP was decomposed into isocyanato intermediate and HQ/BPA molecules, then the isocyanoto intermediate was hydrolyzed into amino groups that were anchored in the molecularly imprinted cavities.

The fact that the two organosilica precursors were incorporated into the framework wall during the co-condensation procedure can also be evidenced by ^{29}Si MAS NMR. In the ^{29}Si spectra of materials of MIMS-HQ (14) and MIMS-BPA (14), five peaks can be observed (**Fig. S2**). The chemical shifts of siloxanes and partially condensed siloxanes are well-known.Two obvious peaks at -60 ppm and -68 ppm for both of the materials can be assigned to T-type organosilica species of T^2 [$RSi(OSi)_2(OH)$] and T^3 [$RSi(OSi)_3$] (R = $-(CH_2)_3-NH_2$). Three peaks at -93 ppm, -102 ppm and -113 ppm respectively can be assigned to Q-type silicon species of Q^2 [$Si(OSi)_2(OH)_2$], Q^3 [$Si(OSi)_3(OH)$] and Q^4 [$Si(OSi)_4$].

The incorporation of HQP/BPAP and the removal of HQ/BPA can also be obviously distinguished from the TG (**Fig. S3**) analysis. It is shown that the mass loss increases from 18% to 25% with the dosage of the organosilica precursors increased for molecularly imprinted materials of MIMS-NHQ and from 16% to 22% for non-imprinted materials of MIMS-HQ. Clearly, more molar ratio of HPQ was used in the material, higher mass loss can be observed. At the same time, the materials of MIMS-NHQ display a higher mass loss than the materials of MIMS-HQ owing to the removal of the imprinting molecules. MIMS-NBPA (14) prepared with larger size of imprinting molecule of BPA gives higher mass loss compared with MIMS-NHQ (14), implying larger volume of imprinted cavities in MIMS-BPA (14) can be formed after removal of the imprinting molecules.

The powder XRD characterization of hybrid materials MIMS-NHQ shows three well-resolved Bragg diffraction peaks in region of 2θ = 0.5~2.3º after removal of the surfactant P123 by solvent extraction of ethanol and concentrated hydrochloric acid that can be indexed as [100], [110], [200] reflections. These reflections are typical for a well-ordered 2D-hexagonal (p6mm) mesostructure. (**Fig. 2**, left). Meanwhile, three reflections on [100], [110], [200] plane in the

range of 2θ =0.5~2.3º for materials of MIMS-HQ can be indexed as the preservation of highly ordered mesostructure after the thermal treatment in solvent of DMSO, as seen in **Fig. 2**, right. Nevertheless,

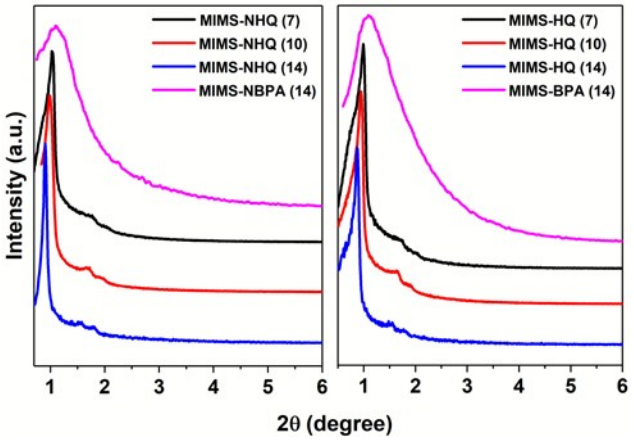

Fig. 2 Powder XRD patterns of the hybrid mesoporous materials of MIMS-NHQ/NBPA (left) and MIMS-HQ/BPA (right)

only one broad diffraction peak in region of 2θ =0.5~3.0º can be observed in the materials of MIMS-NBPA and MIMS-BPA, pointing to a kind of less ordered mesostructure. The absence of [110], [200] reflections indicates limited periodicity in the long range order. One can conclude that varying the imprinting molecule from HQP to BPAP with a larger molecular size broadens the [100] peak and vanishes the [110] and [200] peaks, which suggests that a larger size oforganosilica precursor strongly influenced co-condensation procedure with TEOS and tended to destroy the ordered assembling micelles, and finally resulted in disordered mesostructure. This can be obviously evidenced by the corresponding SEM and TEM images.

The morphology and mesoporous structure of the hybrid mesoporous materials were revealed by SEM and TEM techniques. Based on the SEM images (**Fig. S4**), the morphologies of MIMS-NHQ

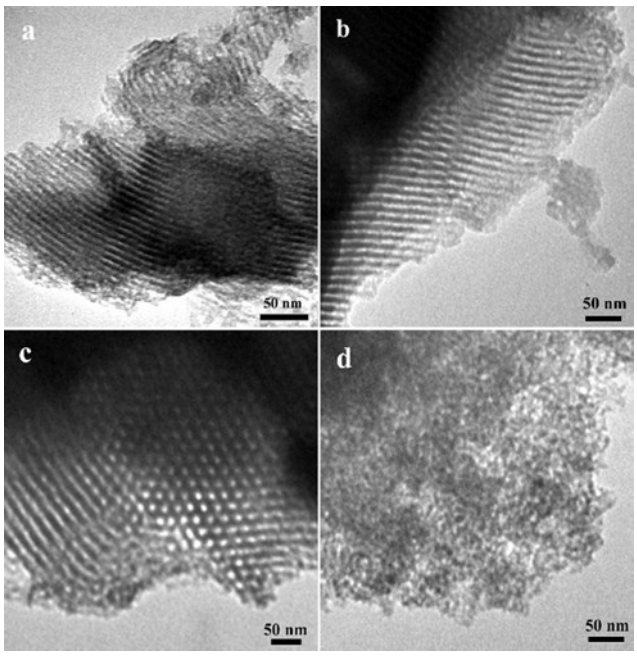

Fig. 3 TEM images of a) MIMS-HQ (7), b) MIMS-HQ (10), c) MIMS-HQ (14) and d) MIMS-BPA (14).

View Article Online
DOI: 10.1039/C7DT04832G

and MIMS-HQ exhibit noodle-like shape with rough surface, whereas MIMS-NBPA and MIMS-BPA possess irregular particles with random shapes. This confirms that a larger size of organosilica precursor strongly influences co-condensation procedure with TEOS, as observed in XRD results. Note that the HQP precursor can be homogeneously incorporated into framework wall of the materials with a uniform morphology even the molar ratio of TEOS and organosilica HQP precursor was decreased to 7. The morphology of the materials could be retained during the procedure of eliminating the imprinting molecules by refluxing in DMSO for 5-6 hours, demonstrating that the framework wall of the materials is robust enough to endure high temperature. At the same time, the energy- dispersive spectroscopy mappings (**Fig. S5**) were taken on the materials of MIMS-NHQ (14), MIMS-HQ (14), MIMS-NBPA (14) and MIMS-BPA (14). It is observed that the N element is uniformly distributed in the framework of all materials, which suggests that the condensation of HQP or BPAP with TEOS randomly occurs.

Transmission electron microscopy (TEM) images (**Fig. 3**) of the hybrid mesoporous materials show the existence of mesopores after removing the surfactant P123. Clearly, MIMS-HQ (7), MIMS-HQ (10) and MIMS-HQ (14) possess ordered hexagonal mesopores, whereas the less ordered worm-like mesopore structure is observed in MIMS-BPA (14). This result indicates that the incorporation of a larger organic groups into the skeleton may destroy the ordered mesostructure, which is in accordance with the XRD results. Additionally, the pore size measured from the TEM images is around 7.2 nm, and this is very close to that calculated

Table 1 Physicochemical properties of the hybrid mesoporous materials

Samples	N content[a] (%)	BET surface area (m^2g^{-1})	Pore diameter[b] (nm)	Pore volume (cm^3g^{-1})
MIMS-NHQ (7)	3.3	536	6.8	0.97
MIMS-HQ (7)	3.4	512	6.9	1.07
MIMS-NHQ (10)	2.4	531	7.7	0.92
MIMS-HQ (10)	2.5	498	7.9	1.05
MIMS-NHQ (14)	2.0	634	6.2	0.76
MIMS-HQ (14)	2.2	623	7.5	0.77
MIMS-NBPA (14)	1.3	430	3.2	0.35
MIMS-BPA (14)	1.6	730	3.4	0.60
SBA-15-APTES	2.33	513	6.2	0.64
SBA-15-APTES-grafted	3.41	288	5.5	0.39

[a] Calculated from the C, H, N elemental analysis.
[b] Calculated from the adsorption branch with the BJH method.

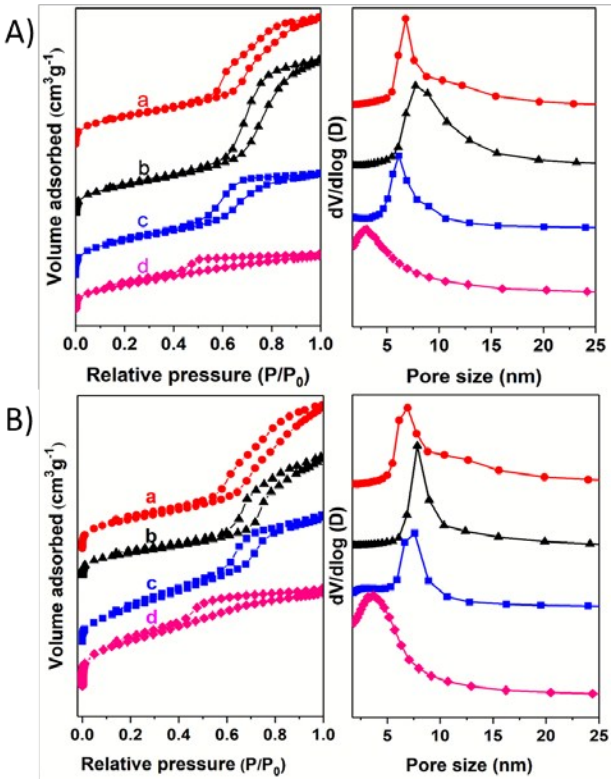

Fig. 4 N_2 adsorption and desorption isotherms (left) and pore size distribution (right) for materials of (a) MIMS-NHQ (7), (b) MIMS-NHQ (10), (c) MIMS-NHQ (14), (d) MIMS-NBPA (14) (A) and (a) MIMS-HQ (7), (b) MIMS-HQ (10), (c) MIMS-HQ (14), (d) MIMS-BPA (14) (B)

from N_2 adsorption test.

The pore size and other physicochemical properties of the hybrid materials were further investigated by N_2 adsorption (**Fig. 4**). For each sample, the adsorption-desorption isotherm shows a type IV curve with H_2-type hysteresis loop at relative pressure P/P_0 region higher than 0.5, which is the typical characteristic of ordered mesoporous materials[44]. **Table 1** displays physical parameters of the hybrid materials. Interestingly, the BET surface area and pore volume increase dramatically in material of MIMS-BPA than those in MIMS-NBPA, implying the formation of molecularly imprinted cavities after the removal of imprinting molecules. Such phenomenon is less pronounced in the cases of MIMS-HQ and MIMS-NHQ. The reason may be that the skeleton of these materials can be shrunk further when heated at 165°C in DMSO, leading to decline of the BET surface. However, larger imprinting molecules facilitate to create larger volume of molecularly imprinted cavities, which can make up for the loss of the BET surface. Obviously, the issue of HQ type materials is inclined to the former factor.

Adsorption of the imprinting molecules

To confirm the presence of molecularly imprinted cavities, adsorption experiments on imprinting molecules were carried out. In view of molecular imprinting polymers can recognize specific substrate in size, shape and functional groups similar to template molecules, these materials were applied as solid-phase extraction absorbent for template molecules hydroquinone and bisphenol A.

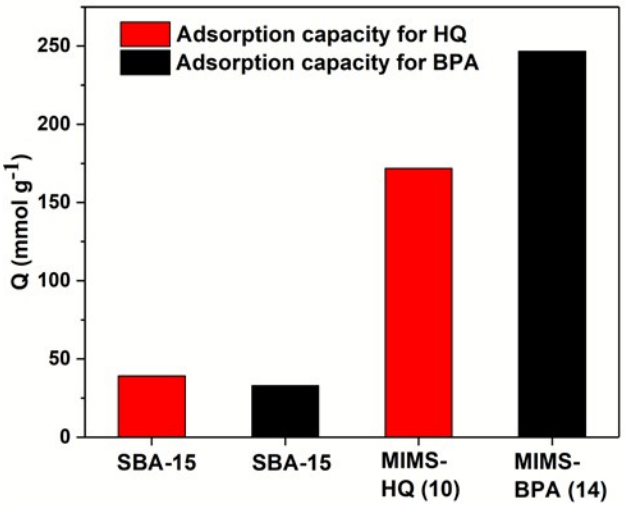

Fig. 5 Adsorption capacity of imprinting molecules HQ and BPA on SBA-15, MIMS-HQ (10) and MIMS-BPA (14)

Based on the UV-vis absorption results, the adsorption capacities of materials MIMS-HQ (14) and MIMS-BPA (14) were calculated as 171.8 μmol g^{-1} and 246.6 μmol g^{-1}, respectively. Meanwhile, the sample of pure SBA-15 just displayed much less adsorption of HQ (39.2 μmol g^{-1}) and BPA (33.0 μmol g^{-1}), as shown in **Fig. 5**. Clearly, the molecularly imprinting cavities were successfully formed after a given thermal treatment.

Catalytic performance

The Knoevenagel reaction of aldehyde is one of the most important and widely used methodology for C-C bond formation in the synthetic field of fine chemical industry as well as biological heterocyclic compounds[45]. Usually, this kind of reaction is catalyzed by weak base chemicals like amines, piperidine and so on. In view of the existence of weak base species of amino groups in our materials, all of these hybrid mesoporous materials were evaluated as heterogeneous catalysts in Knoevenagel reactions and proved to exhibit excellent catalytic activity and selectivity for various aromatic aldehydes. **Table 2** displays the catalytic performance of Knoevenagel reactions about anisaldehyde and ethyl cyanoacetate with different catalysts. For the result of blank reaction, no product formed without catalyst under the condition (entry 1). All of the samples containing N species were active and selective for the reaction, and therefore, N species were active sites for the reactions.

In order to evaluate the basicity of the materials and the accessibility of the N species, CO_2 chemisorption characterization of all the catalysts was carried out and the results are summarized in **Table S1**. It has been reported that the weak chemical interactions between CO_2 and amine groups may play an important role in sorption of CO_2 at 60-90°C. Clearly, all the materials with molecularly imprinted cavities (MIMS-HQ and MIMS-BPA) possess higher absorbed CO_2 amount compared with the corresponding materials containing imprinting molecules in framework (MIMS-

NHQ and MIMS-NBPA). Higher content of CO_2 absorption points to higher basicity of the material and easier accessibility of the N species. Based on such results, amino groups with higher basicity and molecularly imprinted cavities in the mesopore framework are simultaneously created via the thermal treatment in DMSO, which may contribute to the improved performances in Knoevenagel reactions.

Table 2 Catalytic conversion of anisaldehyde employing different catalysts in Knoevenagel reaction[a]

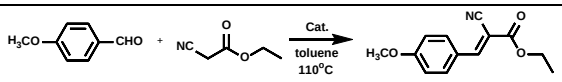

Entry	Catalyst	Conversion (%)[b]	TOF (h^{-1})[c]
1	Blank[d]	□ 1	-
2	MIMS-NHQ (7)	89.5	16.0
3	MIMS-HQ (7)	94.5	23.3
4	MIMS-NHQ (10)	85.5	15.4
5	MIMS-HQ (10)	93.1	24.4
6	MIMS-NHQ (14)	90.4	29.5
7	MIMS-HQ (14)	94.8	30.3
8	MIMS-NBPA (14)	82.3	15.2
9	MIMS-BPA (14)	92.6	35.8

[a] The reactions were carried out in 2 mL of toluene with 40 mg of catalyst at 110oC for 3 hours.
[b] Conversion determined by GC analysis with n-butanol as internal standard substance.
[c] The TOF values were calculated at the reaction time of 20 minutes based on N content of the catalyst.
[d] The blank reaction was performed in the same condition but without any catalyst.

Compared with the materials of MIMS-NHQ/NBPA, MIMS-HQ/BPA materials give higher conversion of anisaldehyde and TOF (number of converted aldehyde molecules per active site per hour) numbers based on the N content in the materials at the reaction time of 20 minutes. Meanwhile, higher initial reaction rates can also be observed on MIMS-HQ/BPA obtained from the conversions of anisaldehyde with different reaction time (**Fig.6**). During the thermal treatment in DMSO, the covalently bonded moieties of –NH-COO- in framework of MIMS materials were decomposed into naked groups of $–NH_2$ in molecularly imprinted cavities, thus the latter will show a better performance in Knoevenagel reaction owing to the increase of basicity.

The TOF value of the reaction catalyzed by MIMS-BPA (14) was also compared with that of MIMS-HQ (14). It can be observed that MIMS-BPA (14) prepared from imprinting molecule (BPA) with larger size give higher TOF number than MIMS-HQ (14) prepared with imprinting molecule HQ. Note here that imprinting molecules with larger size finally results in larger volume of molecularly imprinted cavities. Based on the fact that the basicity of the two materials are similar, the difference of TOF values relies on the void volume of molecularly imprinted cavities. Apparently, the size of

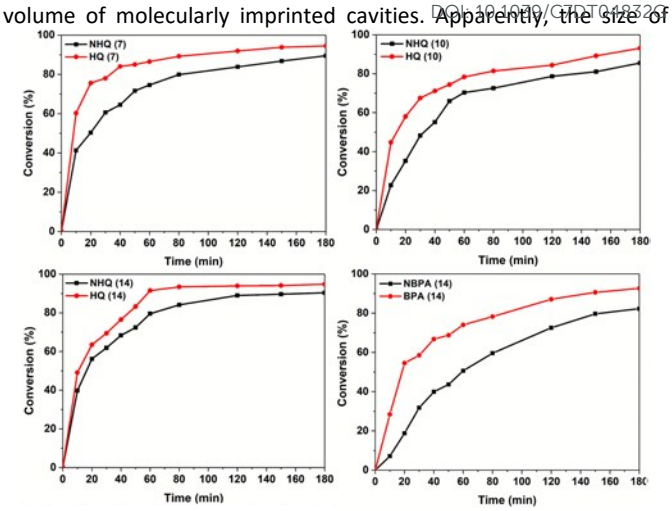

Fig. 6 Catalytic activities in Knoevenagel reaction as a function of reaction time over MIMS-HQ/NHQ and MIMS-BPA/NBPA.

imprinting molecules has an influence on the catalytic TOF values: imprinting molecules with relatively bulkier size tend to lead higher accessibility to the active sites.

In order to prove if the molecularly imprinted cavities facilitate the improvement of activity in the reactions, two control samples (SBA-15-APTES and SBA-15-APTES-grafted) were prepared. SBA-15-APTES was prepared via co-condensation of TEOS and 3-aminopropyltriethoxysilane (APTES) in acid aqueous and SBA-15-APTES-grafted was synthesized through grafting APTES onto the channel of as-prepared SBA-15 material by refluxing in absolute toluene (the detailed synthesis procedure and characterization were displayed in SI). It is well known that a large fraction of amino groups might be located in the mesopores in materials of SBA-15-APTES, which would undermine mass transfer procedure during reactions. Because the amino contents in the materials are quite different, it is more meaningful to compare the TOF values in order to evaluate the superiority of the catalysts. It is remarkable that MIMS-BPA give higher initial reaction rate (67.5 h^{-1}) for the Knoevenagel reaction of 1-naphthaldehyde with cyanoacetate

Table 3 Catalytic conversion and TOF comparison in Knoevenagel reaction 1-naphthaldehyde with different catalysts[a]

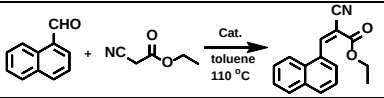

Entry	Catalyst	N content (%)	Conversion[b] (%)	TOF[c]
1	MIMS-BPA (14)	1.6	51.5	67.5
2	SBA-15-APTES	2.33	54.3	48.9
3	SBA-15-APTES-grafted	3.41	89.6	55.2

[a] 1mmol 1-naphthaldehyde and 1 mmol cyanoacetate were dispersed in 2 mL of toluene with 40 mg of catalyst and the reactions were proceeded at 110°C for 10 minutes.
[b] The conversion of aldehyde was calculated by GC analysis with n-butanol as internal standard substrate.

View Article Online
DOI: 10.1039/C7DT04832G

[c] The number of TOF was calculated depending on N content of the catalyst with the result at the reaction time of 10 minutes.

based on the activity at the reaction time of 10 minutes than SBA-15-APTES (48.9 h^{-1}) and SBA-15-APTES-grafted (55.2 h^{-1}), although SBA-15-APTES possesses slightly higher pore volume (0.64 cm^3g^{-1}) compared with MIMS-BPA (0.60 cm^3g^{-1}). The data is displayed in Table 3. By considering that the amino groups anchored in the mesopores might limit the diffusion of the reactants in the mesopore channels, especially in the cases of bulky reactants, the higher initial reaction rate on MIMS-BPA could be ascribed to the higher accessibility of the unblocked active amino groups in the framework via the unblocked mesopore channels as well as the molecularly imprinted cavities. This confirms the advantages of such molecularly imprinted organosilicates applied in catalysis.

The mechanism of Knoevenagel condensation is generally accepted that the reaction proceeds through the proton abstraction of active methylene compounds[46, 47]. The activation of methylene group is the key step for the proceeding of the reaction. Based on all of the above characterizations and analysis, the reaction process in the mesopore channels of the catalysts is shown in **Scheme 3**. It is assumed that the cyanoacetate and aldehyde diffuse into the mesopore channels of the materials and reach the active amino groups. Such base amino groups would take a proton from the methylene group in cyanoacetate and then negative charged cyanoacetate would attack the carbonyl group in aldehyde to form negative oxygen type intermediate. Finally, the protonated base would neutralize the intermediate, so the neutralized base can be active in the next run of catalysis to boost the reaction going fluently. Note here that the introduction of ordered mesopores into molecule imprinting materials improves the accessibility of active species.

In order to assess the recyclability potential of such mesoporous materials and the stability of amino groups in the framework wall, recycling experiments were carried out with MIMS-HQ (14) as a model catalyst over the substrate anisaldehyde. **Fig. 7** shows the results of the recycled catalyst of MIMS-HQ (14) after five-times recycling by washing with ethanol for three times (Runs 2 and 3) and regenerating under nitrogen atmosphere (Run 4-6). In the former cases, the conversion of anisaldehyde in Knoevenagel reaction with ethyl cyanoacetate gradually decreased in repeated runs, which is possibly due to the deposition of reaction residues on the active amino groups in the framework wall or the leaching of amino groups during the reaction. An alternative way to regenerate the catalyst is via intermediate calcination at 200°C for 2 hours at inert atmosphere. Under such treatment, the amino groups exposed in the cavities of the catalyst are almost preserved, as

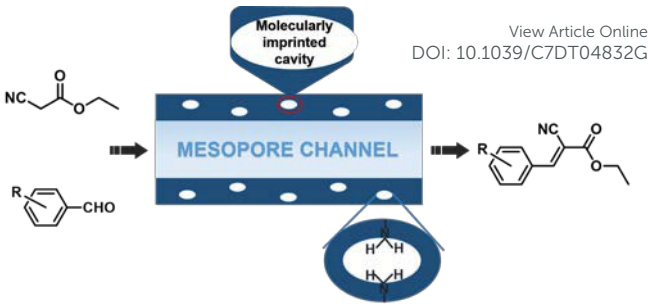

Scheme 3 Catalytic procedure for Knoevenagel reaction

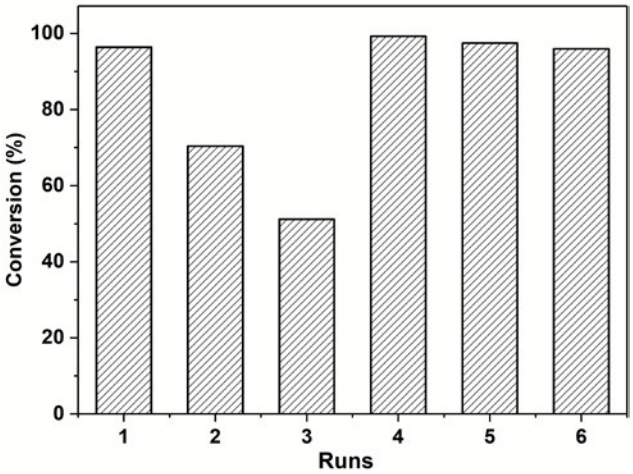

Fig. 7 Catalytic activity of repeated use of MIMS-HQ (14) in the Knoevenagel reaction of anisaldehyde and ethyl cyanoacetate by washing (Run 2&3) and intermediate calcination (Run 4-6) approaches.

evidenced by the FT-IR spectrum of the material after calcination (**Fig. S8**). The almost complete reactivation of the recycled MIMS-HQ (14) was achieved by the intermediate calcination treatment (Run 4), giving comparable conversion as that in Run 1. Therefore, the gradual reduced catalytic conversion for anisaldehyde in the washing cases is mainly due to deposition of residues on the active amino groups because they may hinder the access of reagents to the active amino groups, however, which would be vanished during the intermediate calcination procedure. The conversion of anisaldehyde was almost constant in Runs 4-6, suggesting that the intermediate calcination at 200°C for 2 hours at inert atmosphere is an effective way to regenerate MIMS-HQ (14) in the Knoevenagel reactions and that the stability of the amino groups in the framework wall is high.

One of the benefits of MIMS-BPA (14) is represented by the molecularly imprinted cavities in the mesoporous framework. To investigate if this effect is limited to anisaldehyde, MIMS-BPA (14) was tested for the Knoevenagel reactions of other aldehydes, such as formylofuran, benzaldehyde and 1-naphthaldehyde (as shown in **Table S2**). Clearly, MIMS-BPA (14) proved to be catalytically active in all reactions tested, which indicates that this kind of material fit to catalyze various reactants. These results further confirmed the advantage of the molecularly imprinted cavities in the mesopore framework.

Conclusions

In summary, hybrid molecularly imprinted mesoporous materials of MIMS-NHQ/NBPA were successfully fabricated via co-condensation of TEOS and alkoxysilane precursors by a triblock copolymer-templated sol-gel approach. The imprinting molecules of HQ and BPA were introduced in the alkoxysilane precursor via a thermally reversible covalent bond by linking an imprinting molecule to a functional alkoxysilane monomer. After a given thermal treatment, amino groups with higher basicity and molecularly imprinted cavities were simultaneously formed in the mesoporous framework wall. Such hybrid mesoporous materials were then used to catalyze heterogeneous Knoevenagel reactions. As expected, the materials with molecularly imprinted cavities gave higher catalytic conversion and TOF number compared with the materials with imprinting molecules due to the combined advantages of active sites with higher basicity and molecularly imprinted cavities.

The role of molecularly imprinted cavities in leading to improved accessibility of the catalytic amino groups in the framework wall was confirmed by comparing the conversions with two control samples (SBA-15-APTES and SBA-15-APTES-grafted). It was found that the size of imprinting molecules has an influence on the catalytic conversion and TOF values, that is, imprinting molecules with relatively bulkier size tend to higher accessibility to the active sites. Finally, this work provides a new way to realize extended exposure of active organic species in the mesoporous framework wall through the creation of cavities nearby the active sites.

Acknowledgements

This work was supported by National Natural Science Foundation of China (51472062) and the Opening Project of Key Laboratory of Polyoxometalate Science of Ministry of Education.

Notes and references

1. L. Wang, J. Zhang, X. Yi, A. Zheng, F. Deng, C. Chen, Y. Ji, F. Liu, X. Meng and F.-S. Xiao, *ACS Catal.*, 2015, **5**, 2727-2734.
2. L. Li, D. Cani and P. P. Pescarmona, *Inorg. Chim. Acta*, 2015, **431**, 289-296.
3. D. Li, L. Zeng, X. Li, X. Wang, H. Ma, S. Assabumrungrat and J. Gong, *Appl. Catal. B: Environmental*, 2015, **176-177**, 532-541.
4. W. Fu, L. Zhang, D. Wu, M. Xiang, Q. Zhuo, K. Huang, Z. Tao and T. Tang, *J. Catal.*, 2015, **330**, 423-433.
5. N. Lu, Y. Tian, W. Tian, P. Huang, Y. Liu, Y. Tang, C. Wang, S. Wang, Y. Su, Y. Zhang, J. Pan, Z. Teng and G. Lu, *ACS Appl Mater. Interfaces*, 2016, **8**, 2985-2993.
6. R. Ran, L. You, B. Di, W. Hao, M. Su, F. Yan and L. Huang, *J. Sep. Sci.*, 2012, **35**, 1854-1862.
7. K. Sim, N. Lee, J. Kim, E. B. Cho, C. Gunathilake and M. Jaroniec, *ACS Appl. Mater. Interfaces*, 2015, **7**, 6792-6802.
8. H.-T. Chen, S. Huh, J. W. Wiench, M. Pruski and V. S.-Y. Lin, *J. Am. Chem. Soc.*, 2005, **127**, 13305-13311.
9. Y. Wei, X. Li, A. A. Elzatahry, R. Zhang, W. Wang, X. Tang, J. M. E. Davis, *J. Am. Chem. Soc.*, 2008, **130**, 13442–13449.
10. F. Hoffmann, M. Cornelius, J. Morell and M. Froba, *Angew. Chem. Int. Ed*, 2006, **45**, 3216-3251.
11. S. Rostamnia, E. Doustkhah, R. Bulgar and B. Zeynizadeh, *Microporous Mesoporous Mater.*, 2016, **225**, 272-279.
12. S. S. Park, M. S. Moorthy and C.-S. Ha, *Korean J. Chem. Eng.*, 2014, **31**, 1707-1719.
13. M. von der Lehr, C. F. Seidler, D. H. Taffa, M. Wark, B. M. Smarsly and R. Marschall, *ACS Appl. Mater. Interfaces*, 2016, **8**, 25476-25488.
14. X. Wu, L. You, B. Di, W. Hao, M. Su, Y. Gu and L. Shen, *J. chromatogr.. A*, 2013, **1299**, 78-84.
15. X. Liu, P. Wang, L. Zhang, J. Yang, C. Li and Q. Yang, *Chemistry*, 2010, **16**, 12727-12735.
16. Q. Yang, D. Han, H. Yang and C. Li, *Chemistry, an Asian journal*, 2008, **3**, 1214-1229.
17. C. Baleizao, B. Gigante, D. Das, M. Alvaro, H. Garcia and A. Corma, *J. Catal.*, 2004, **223**, 106-113.
18. Y.-J. Li, L. Wang and B. Yan, *J. Mater. Chem.*, 2011, **21**, 1130-1138.
19. M. Wu, Q. Meng, Y. Chen, Y. Du, L. Zhang, Y. Li, L. Zhang and J. Shi, *Adv. Mater.*, 2015, **27**, 215-222.
20. S. H. Lee, S. S. Park, S. Parambadath and C.-S. Ha, *Microporous Mesoporous Mater.*, 2016, **226**, 179-190.
21. D. Herault, G. Cerveau, R. J. P. Corriu, A. Mehdi, *Dalton Trans.*, 2011, **40**, 446-451.
22. E. L. Margelefsky, A. Bendje´riou, R. K. Zeidan, V. r. Dufaud and Yang, J. Wang, D. Al-Dahyan and D. Zhao, *RSC Adv.*, 2016, **6**, 51470-51479.
23. J. Alauzun, A. Mehdi, C. Reye´, R. J. P. Corriu, *J. Am. Chem. Soc.*, 2006, **128**, 8718-8719.
24. Z. Zhou, F. Piepenbreier, V. R. R. Marthala, K. Karbacher and M. Hartmann, *Catal. Today*, 2015, **243**, 173-183.
25. N. K. Mal, M. Fujiwara and Y. Tanaka, *Nature*, 2003, **421**, 350-353.
26. Y. L, Y. Jiang, Z. Ruan, K. Lin, Z. Yu, Z. Zheng, X. Xu and Y. Yuan, *J.Mater. Chem. A*, 2017, **5**, 21300-21312.
27. L. Qin, W. Shi, W. Liu, Y. Yang, X. Liu and B. Xu, *Rsc Adv.*, 2016, **6**, 12504-12513.
28. Y. Chen, D. Li, Z. Bie, X. He and Z. Liu, *Anal. Chem.*, 2016, **88**, 1447-1454.
29. C. Li, H. Zhang, D. Jiang and Q. Yang, *Chem. Commun.*, 2007, **0**, 547-558.
30. S. Roy, P. Bhanja, S. Safikul Islam, A. Bhaumik and S. M. Islam, *Chem. Commun.*, 2016, **52**, 1871-1874.
31. S. Xiang, Y. Zhang, Q. Xin and C. Li, *Angew. Chem. Int. Ed.*, 2002, **41**, 821-824.
32. T. Cheng, Q. Zhao, D. Zhang and G. Liu, *Curr.Org.Chem.*, 2015, **19**, 667-680.
33. C. Tourné-Péteilh, D. Brunel, S. Bégu, B. Chiche, F. Fajula, D. A. Lerner and J.-M. Devoisselle, *New J. Chem.*, 2003, **27**, 1415-1418.
34. N. K. Mal, M. Fujiwara, Y. Tanaka, T. Taguchi and M. Matsukata, *Chem. Mater.*, 2003, **15**, 3385-3394.
35. D. Jiang, Q. Yang, J. Yang, L. Zhang, G. Zhu, W. Su and C. Li, *Chem. Mater.*, 2005, **17**, 6154-6160.
36. S. Muratsugu, N. Maity, H. Baba, M. Tasaki and M. Tada, *Dalton Trans.*, 2017, **46**, 3125-3134.
37. Y. Yang, Z. Weng, S. Muratsugu, N. Ishiguro, S. Ohkoshi and M. Tada, *Chem. Eur. J.*, 2012, **18**, 1142-1153.
38. J. Yin, Y. Cui, G. Yang and H. Wang, *Chem. Commun.,* 2010, **46**, 7688-7690.
39. M. Ravera, E. Gabano, I. Zanellato, E. Perin, A. Arrais and D. Osella, *Dalton Trans.*, 2016, **45**, 17233-17240.
40. R. N. Liang, D. A. Song, R. M. Zhang and W. Qin, *Angew. Chem.*

View Article Online
DOI: 10.1039/C7DT04832G

Int. Ed., 2010, **49**, 2556-2559.
41. A. Bogomolova, E. Komarova, K. Reber, T. Gerasimov, S. B. O. Yavuz and M. Aldissi, *Anal. Chem.*, 2009, **81**, 3944–3949.
42. E. Besson, A. Mehdi, A. Van der Lee, H. Chollet, C. Reye, R. Guilard, R. J. P. Corriu, *Chem. Eur. J.*, 2010, **16**, 10226-10233.
43. J. E. Lofgreen, I. L. Moudrakovski and G. A. Ozin, *ACS Nano*, 2011, **5**, 2277-2287.
44. Y. Wei, X. Li, R. Zhang, Y. Liu, W. Wang, Y. Ling, A. M. El-Toni and D. Zhao, *Sci. Rep.*, 2016, **6**, 20769.
45. L. F. Tietz, *Chem. Rev*., 1996, **96**, 115-136.
46. C. Cope, *J. Am. Chem. Soc.*, 1937, **59**, 2327-2330.
47. W. Notz, F. Tanaka, C. F. Barbas, *Acc. Chem. Res.* 2004, **37**, 580-591.